CONF-8508153--2

NEUTRON POWDER DIFFRACTION AT A PULSED NEUTRON SOURCE: A STUDY OF RESOLUTION EFFECTS*

J. Faber, Jr. and R. L. Hitterman
Materials Science and Technology Division
Argonne National Laboratory
Argonne, IL 60439

CONF-8508153--2

DE86 005548

FINAL

November 1985

DISCLAIMER

MASTER

Invited paper to be published in Advances in X-ray Analysis, Vol. 29, Proceedings of the 34th Annual Denver X-ray Conference, held in Snowmass, CO, August 5-9, 1985.

*Work supported by the U. S. Department of Energy, BES-Materials Sciences, under Contract W-31-109-Eng-38.

NEUTRON POWDER DIFFRACTION AT A PULSED NEUTRON SOURCE: A STUDY OF RESOLUTION EFFECTS*

J. Faber, Jr. and R. L. Hitterman
Materials Science and Technology Division
Argonne National Laboratory
Argonne, IL 60439

FINAL

November 1985

Invited paper to be published in Advances in X-ray Analysis, Vol. 29, Proceedings of the 34th Annual Denver X-ray Conference, held in Snowmass, CO, August 5-9, 1985.

*Work supported by the U. S. Department of Energy, BES-Materials Sciences, under Contract W-31-109-Eng-38.

NEUTRON POWDER DIFFRACTION AT A PULSED NEUTRON SOURCE: A STUDY OF RESOLUTION EFFECTS.

J. Faber, Jr. and R. L. Hitterman

Argonne National Laboratory
Materials Science and Technology Division
Argonne, IL, 60439

ABSTRACT

The General Purpose Powder Diffractometer (GPPD), a high resolution ($\Delta d/d=0.002$) time-of-flight instrument, exhibits a resolution function that is almost independent of d-spacing. Some of the special properties of time-of-flight scattering data obtained at a pulsed neutron source will be discussed. A method is described that transforms wavelength dependent data, obtained at a pulsed neutron source, so that standard structural least-squares analyses can be applied. Several criteria are given to show when these techniques are useful in time-of-flight data analysis.

I. INTRODUCTION

The GPPD is a high resolution time-of-flight (TOF) neutron scattering instrument at the Argonne Intense Pulsed Neutron Source (IPNS). The IPNS[1,2] is a major user-dedicated national facility that produces pulsed beams of polychromatic neutrons in the thermal regime ($0.15<\lambda<15$Å). Neutrons are produced by spallation using a uranium target and 450MeV protons. By pulsing the proton accelerator at 30Hz, the neutrons are produced in short bursts. For scattering studies in the thermal regime[3], the fast neutrons produced by spallation are slowed-down by hydrogenous moderator materials (typically polyethylene or liquid methane) to provide

white beam thermalized neutron fluxes. The time for a neutron to be emitted from the moderator varies approximately as 1/v, where v is the neutron velocity. The width of the pulse thus varies from about 5 to 50μs and depends upon the moderator effective temperature and geometry, and the neutron energy, or corresponding wavelength. As we shall see (Section II), steady state methods that require scattering angle scans are replaced with scans in TOF, at constant angle.

In this paper, we shall briefly describe the configuration of the GPPD at IPNS (Section III). In particular, we shall show how high data acquisition rates and high resolution can be realized in the TOF case. To emphasize the high resolution capability of the GPPD, a transformation of the TOF data will be described that takes into account the special wavelength dependent properties of TOF data obtained from a pulsed neutron source (see Section IV). This particular transformation however, does not obviate the need to recover precise integrated intensity information from the transformed data. We have written a computer code, TOFMANY, that is designed to recover integrated intensity information from TOF data at IPNS. This method is of particular importance when standard Rietveld[4] techniques cannot adequately fit the Bragg profiles. For materials with very complicated crystal structures, the choice of techniques for structural refinement become severely limited. Analysis methods that rely on single peak or multiplet peak measurement techniques must be abandoned, but the Rietveld structure refinement technique[5,6] is available.

II. SEVERAL USEFUL TOF RELATIONS

For crystalline samples, the information about interplanar spacings can be obtained by rewriting Bragg's law in terms of t, the time of flight required for a neutron to travel the total flight path L, from source to detector:

$$\lambda=h/mv=ht/mL=2d\sin\theta, \qquad (1)$$

where d is the interplanar spacing, λ is the neutron wavelength, h is Planck's constant and m is the neutron mass. Equation (1) simplifies to

$$3956t/L=2d\sin\theta, \qquad (2)$$

where t is the time in seconds and L is the total flight path in meters. In the TOF technique, d-space dependent information is obtained by fixing the scattering angle and using standard timing techniques to "scan" TOF. To maximize the efficiency of data acquisition, a very wide wavelength range is desired so that all d-spaces of interest are scanned for each pulse. This is indeed the case for the GPPD at IPNS, where with a room temperature polyethylene moderator, we are able to obtain $0.2<\lambda<5$Å. In the case of steady state techniques, the data acquisition systematics generally involve a scan from low 2θ to high 2θ, or from large to small d-spacing. Notice (see Equations (1) and (2)) that the data are inverted in the TOF case, i.e., a logical organization of the data is from short to long time after each neutron source burst. In this case, the scan is from small to large d-space.

III. THE GPPD AT IPNS

A schematic diagram of the GPPD at the IPNS facility is illustrated in Figure 1. The distance between the source and the sample is 19.96m. Each of the 144 detectors in this instrument is a 10atm ^{3}He gas-filled cylindrically-shaped proportional counter with 1.27cm diameter and 38.1cm long. Detectors are located at various scattering angles but the scattered flight path for all detectors is fixed at 1.5m from the sample position. Standard timing electronics are sufficient to provide a high degree of wavelength resolution in the TOF case. For example, from Equation (2), the velocity for a neutron with λ=1Å is approximately 4000m/s. The standard data acquisition[7,8] timing electronics for the GPPD at IPNS uses an 8MHz clock, which implies roughly 125ns timing resolution. For neutron path lengths illustrated here, the electronic timing resolution is more than adequate. The sample chamber is 2ft in diameter, thus providing sufficient space for ancillary equipment[9].

When compared to x-ray techniques, neutron experiments are almost always considered to be flux-limited. This potential disadvantage in the case of neutrons can be minimized by designing detector banks with large solid angles to optimize data rates. In the case of the GPPD, banks of detectors are located symmetrically on both sides of the incident beam at 2θ=150, 90, and 60°. Separate single detector banks are located at 30 and 20°. Twice the data rate is realized by simply adding the data together from symmetrical detectors on both sides of the instrument. Within a particular bank of detectors, the TOF values for a particular d-spacing

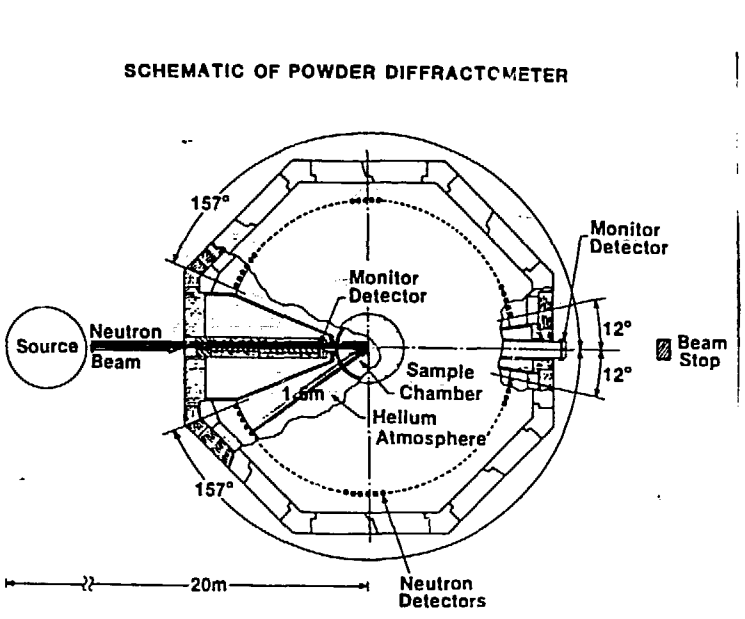

Figure 1. Schematic diagram of the General Purpose Powder Diffractometer (GPPD) at IPNS. Currently there are 144 detectors arranged into eight different scattering angle banks.

or Bragg peak with Miller indices hkl, appear at slightly different TOF values (Equation 2). For the GPPD, this problem is solved with electronic time-focussing of the data[10].

The time-focussing condition, which is essentially a constant $Q=4\pi\sin\theta/\lambda$ requirement can be expressed as:

$$t'=t_i\sin\theta_o/\sin\theta_i, \qquad (3)$$

where t' is the time-focussed time-of-flight value for a neutron event at a detector with Bragg angle θ_i. The reference angle for the entire group of detectors in the bank is defined by θ_o. This means that after the time-focussing algorithm has been applied to each neutron event, a single histogram (neutron intensity vs time-of-flight) representing the collective bank of detectors is obtained. The data acquisition rate is then proportional to the number of detectors in a particular detector bank. One practical limit on solid angle for each detector group and hence count rate for the time-focussed group of detectors is set by desired requirements of acceptable resolution. The scattering angle dependent component of the resolution function of the instrument is proportional to $\cot\theta d\theta$. For example at $2\theta=150°$, as the solid angle of the bank is extended to smaller scattering angles, significant reductions in resolution must be obtained. The present detector complement at $2\theta=150°$

is 31 on each side of the instrument, which spans a total solid angle of 0.13 steradians. There are 144 detectors in the diffractometer. Cost considerations are still the limiting constraint on detector complement, not resolution considerations. For the configuration of detectors at $2\theta=150°$, the time-focussed data rate is roughly 60 times that for a single detector.

The beam size for the GPPD at the sample position has rectangular cross section, 1.27cm wide and 5cm high (samples with cylindrical geometry that match these dimensions are typically used). The neutron absorption cross section for most elements is much smaller than the appropriate quantity for x-rays. If the quantity of available sample is not restrictive, the full beam cross section can be employed, thus providing for substantial increases in neutron data rate. A typical sample might require 4-24 hours of data collect time to produce one histogram (intensity vs TOF) for each of the time-focussed banks of detectors.

In Figure 2, the resolution $\Delta d/d$ at fwhm is shown as a function of $Q=4\pi\sin\theta/\lambda$. The first curve marked in the legend of the figure is the experimentally determined resolution obtained for Cu Kα radiation from a sealed x-ray tube using a standard GE x-ray diffractometer with a 1° beam slit, a 0.1° scattered beam slit and a 4° take-off angle. Notice that with Cu radiation, the maximum $Q_{max}=8\text{Å}^{-1}$. For Mo radiation, the limitations on large Q values are less severe and $Q_{max}\sim 18\text{Å}^{-1}$. In either of these cases, the K-edge involves a doublet of characteristic lines. For the two other resolution examples in Figure 2, this is not the case.

The second curve marked in the legend of Figure 2 is that for the D1A powder diffractometer at the ILL, with $\lambda\sim 1.1$Å. The minimum value of the instrumental resolution function is determined by the take-off angle of the incident beam monochromator. The Q dependence of the resolution function is controlled mainly by the angular divergences in various parts of the beam path. The D1A instrument has an additional degree of versatility in that the take-off angle on the monochromator can be adjusted at will. The minimum of the resolution function can then be tuned to a particular experiment. The last curve listed in the legend is that for the 150° scattering angle bank of the GPPD at IPNS. Notice the enormous Q range spanned by the instrument. The resolution of this instrument is roughly independent of TOF. This can be understood (see Section I) by considering that the source pulse shape widens as 1/v, so that resolution, $\Delta t/t=\Delta d/d=$constant. In practice there are other moderator-dependent contributions to the instrumental resolution

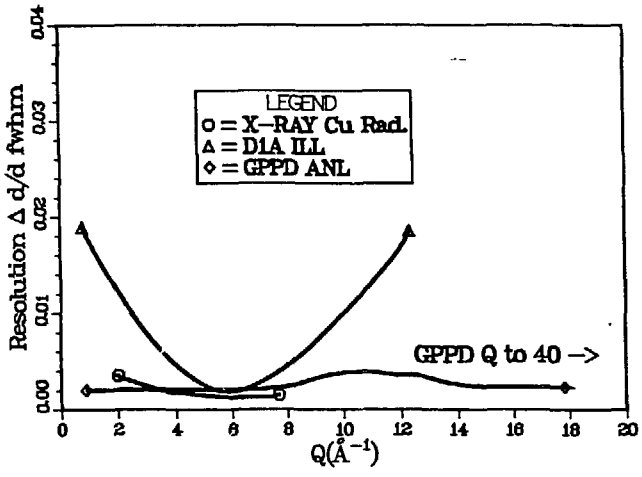

Figure 2. Resolution, Δd/d at full width at half maximum, as a function of $Q=4\pi\sin\theta/\lambda$. The first curve denoted in the legend describes the resolution for a standard x-ray powder diffractometer. The experimental data used to generate a smooth curve provide the low-Q limit shown. The second curve in the legend is for D1A, the high resolution powder diffractometer at the ILL. The last curve described is that for the GPPD at IPNS. Notice the enormous Q range available on this instrument.

function, but these and other particular details of the instrument will be discussed elsewhere. It should be emphasized that neutron scattering lengths as opposed to x-ray atomic scattering factors, f(Q), are scalars. This means that for high resolution neutron powder diffractometers, only thermal vibration effects attenuate the Bragg signal at high Q.

One unique feature of the GPPD is that excellent resolution is obtained at large d-spacings. Standard x-ray methods to measure small strain values emphasize back-scattering or large scattering angle measurements. For a steady state instrument that uses an incident beam monochromator, the emphasis is on Bragg reflections at or near the take-off angle minimum in the resolution function. The corresponding d-space values are intermediate ones. With reasonable freedom to choose the incident beam wavelength, this restriction becomes less severe. In the TOF case, the best strain resolution is obtained at large d-space values. As discussed above, the resolution is approximately independent of d-space and the usual systematics for accumulating data is with constant bin widths in the histogram. At large d values, the density of data points that describe a Bragg peak are largest, thus providing the best

strain resolution. As we shall see in the next section, one disadvantage in the TOF case is that the flux-on-sample for largest d values is low. Thus the time required to achieve acceptable statistics is increased.

IV. RECONSTRUCTION OF TOF DATA FOR STANDARD LEAST-SQUARES ANALYSIS

We begin by noting the expression for the intensity of a powder diffraction Bragg peak using the TOF method:

$$P(hkl)=\phi(\lambda)\eta(\lambda).(\lambda^4/8\pi r).l_s V.(\rho'/\rho).jN^2|F^2|A(hkl)E(hkl)LP(\theta). \quad (3)$$

The incident beam neutron flux is described by $\phi(\lambda)$, $\eta(\lambda)$ is the wavelength dependence of the detector efficiency, r is the distance between sample and detector, l_s is the length of the detector, V is the volume of the sample in the neutron beam, ρ is the density, j the powder multiplicity for the hkl of interest, N is the number density of unit cells illuminated by the beam, F is the structure factor, A(hkl) is the absorption correction, E(hkl) is the extinction correction, and LP(θ) is the Lorentz factor. This expression clearly reflects the λ or TOF relationship between Bragg integrated intensity and the structure factors, F. Note that unlike the usual steady state relation, we must now consider the flux on sample quantity, $\phi(\lambda)$, and the wavelength dependence of the detector efficiency, $\eta(\lambda)$. Figure 3 illustrates the wavelength

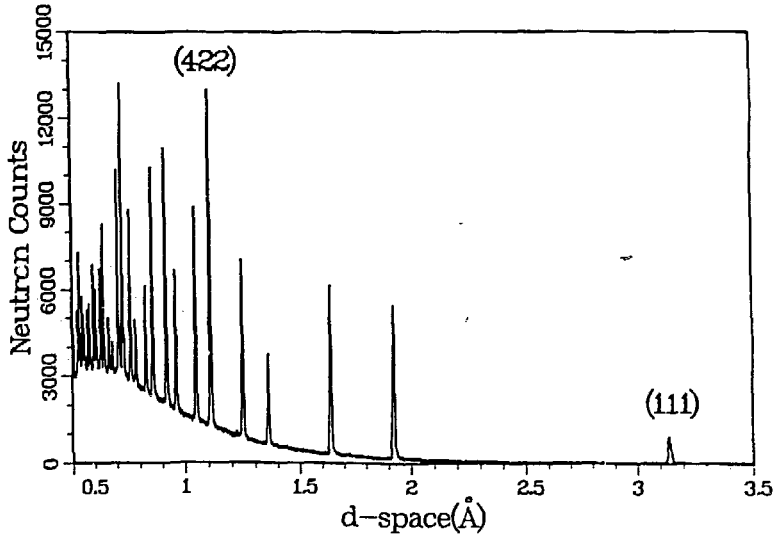

Figure 3. Raw data plot of neutron counts as a function of d-space for a silicon powder sample (2θ=90° detector bank).

dependence of the TOF data from a pulsed neutron source. The data are from the 90° scattering angle banks of the GPPD. The nominal resolution, $\Delta d/d=0.0045$. If we can measure $\phi(\lambda)$ and $\eta(\lambda)$, and correct the data for the λ^4 dependence, then we can extract a quantity that is simply proportional to the structure factors, F. This is accomplished by a separate experiment that measures the scattering from a calibrated vanadium sample (to obtain the product of $\phi(\lambda)$ and $\eta(\lambda)$). The scattering from vanadium is dominated by incoherent scattering[11] (4.8 barns) and therefore produces a constant cross section (neglecting multiple scattering and absorption effects) as a function of TOF. The vanadium Bragg peaks make only a miniscule contribution to the total scattering (the scattering length for vanadium[11], $b_v=-0.04 \times 10^{-8}$ cm while typical scattering lengths are 10-30 times greater than this value and intensity is proportional to b^2). We can construct a simple transformation that renormalizes the data in Figure 3 to remove these wavelength dependent features. Figure 4 shows the results of this transformation. Apart from the λ^4 dependence given in Equation (3), the data in Figure 4 now have an appearance similar to that associated with standard steady state techniques. A standard crystallographic least-squares program can then be used to refine structural parameters. However, in the case of overlapped reflections, it is useful to develop a technique to recover the

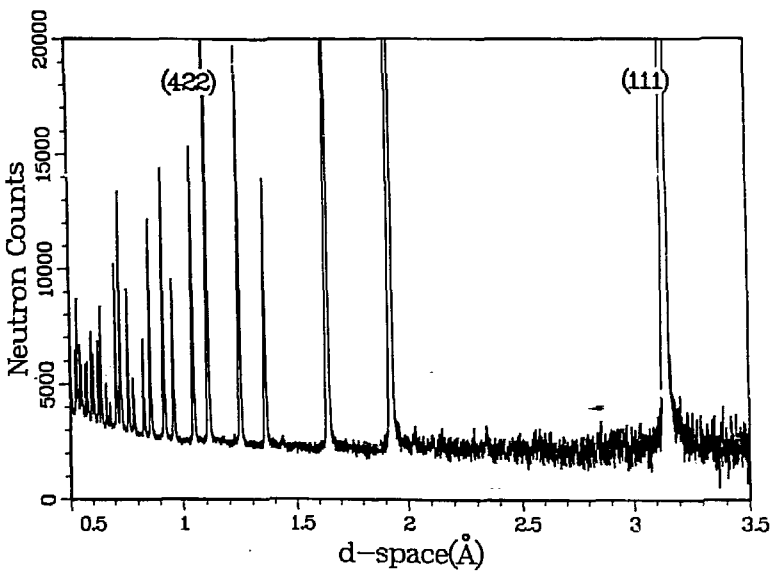

Figure 4. Renormalized data plot of neutron counts as a function of d-space. Vanadium data (not shown) were used to perform a point-by-point renormalization of the data shown in Figure 3. The apparent scatter in the data at large d-space is due to the multiplicative character of the transformation.

integrated intensities of the individual profiles.

A computer code was written to fit multiplets of Bragg profiles using the transformed data illustrated in Figure 4 as input. This code has been successfully used to study the effects of grain interaction stresses[12] in metallurgical samples. The assumption is that the background is reasonably well-determined on both sides of the multiplets. A linear background function is assumed in the TOF region of the multiplet. Figure 4 shows that these assumptions appear reasonable. A moderate degree of structural complexity is accommodated by using this code to analyze partially overlapped Bragg reflections. The integrated intensities of the Bragg reflections are thus obtained. The results are illustrated in Figure 5, where we plot the integrated intensities as a function of $h^2+k^2+l^2$, which is proportional to Q^2, where $Q=4\pi\sin\theta/\lambda$. The very weak $h+k+l=4n+2$ reflections were not analyzed. A correction for absorption has been applied to the data. Note that 48 independent Bragg integrated intensities were obtained from the data illustrated in Figure 4 using TOFMANY to help resolve the partially overlapped reflections at high Q. Rietveld[4] profile refinement analysis was also carried out on the data illustrated in Figure 3. The Rietveld results[5] gave a weighted profile

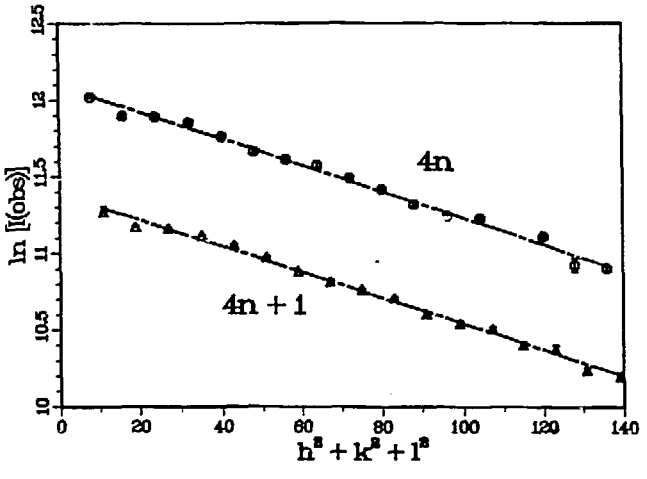

Figure 5. The ln[I(obs)] vs $h^2+k^2+l^2$. Note that $h^2+k^2+l^2 \propto Q^2$. The integrated intensities were obtained from the data illustrated in Figure 4, using the TOFMANY computer code. The very weak $h+k+l=4n+2$ reflections were not analyzed.

residual R_{wtp}=0.031; the silicon temperature factor B(Si)=0.43(1)Å^2 and the lattice parameter, a_o=5.4309(1). Using the data in Figure 5, R(F^2)=0.023 and B(Si)=0.45(1)Å^2. The results are equivalent.

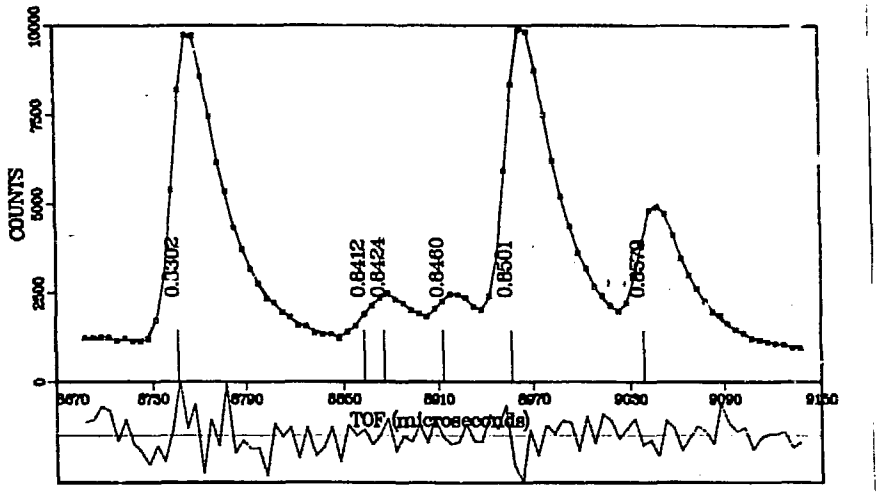

Figure 6. Point by point observed and calculated neutron intensities for a multiplet of six Bragg reflections from Al_2O_3 using the 150° detector bank of the GPPD. The raw data are marked by symbols and the solid line represents the calculated value. The vertical tick marks locate the calculated positions of the peaks in d-space coordinates. The differences between theory and experiment are illustrated in the bottom of the figure. The scale is chosen so that the largest difference fills the allotted vertical space (±300 neutron counts).

Another example of multiplet peak fitting program performance is illustrated in Figure 6. The data are from Al_2O_3. A selected TOF range from the 2θ=150° detector banks was chosen. For the TOF range illustrated, a total of six Bragg reflections were detected. The d-spacings for the Bragg reflections are marked by ticks in Figure 6. For the multiplet fitting results, a measure of goodness of fit can be defined by:

$$\chi^2=\Sigma(\Delta I^2)/N \qquad (4)$$

where ΔI is the weighted differences between theory and experiment, summed over all data points, and N is the number of degrees of freedom of the system (the difference between the the number of observations and the number of adjustable parameters). The results illustrated in Figure 6, gave χ^2=1.3. A question might be raised here concerning the significance

of the fit for a 6-peak fit in the TOF range illustrated in Figure 6. To answer this question, least-squares analysis was carried out using five peaks in the TOF region illustrated in Figure 6. In this case, χ^2=1.8 was obtained. The fit was clearly not of the quality illustrated in Figure 6. Alternatively, when a multiplet of seven reflections was used in the analysis, convergence was not achieved. From a Rietveld analysis of the entire TOF range, integrated intensities of these reflections were obtained. A comparison of the Rietveld and TOFMANY results are shown in Table 1. The intensity values indicate excellent agreement between the methods. Values for the d-spaces for the reflections were also determined in the analysis.

Table 1. Integrated intensity comparison for a multiplet of six Bragg reflections from Al_2O_3. The intensities are normalized to the strongest reflection in this multiplet (see Figure 6). The Miller indices of the reflections correspond to a hexagonal unit cell representation. Estimated standard deviations for the Rietveld-determined integrated intensities were not given in the analysis.

hkl	d-space(Å)	I(Rietveld)	I(TOFMANY)
(4,1, 6)	0.8302(2)	955	984(10)
(2,1,13)	0.8412(2)	81	101(21)
(3,2, 7)	0.8424(4)	107	67(20)
(2,0,14)	0.8460(2)	145	136(3)
(3,0,12)	0.8501(2)	1000	1000(4)
(1,3,10)	0.8579(2)	428	430(4)

V. DISCUSSION

The method to recover the integrated intensities of Bragg peaks described above has several other important applications in powder diffraction studies. Suppose the structure of the material is unknown. Our multiplet fitting program can still be used as an analytic tool to determine the d-spacings of the Bragg lines present in the pattern. Indexing programs that attempt to assign unit cell size and shape can then be tried. The results of a preliminary study to solve the structure of FeOCl intercalated with TTF are available[1,13]. Consider for example particle size, anisotropic strain[12], compositional inhomogeneity, complex polycrystalline texture, and multi-phase metallurgical effects[14]. All of

these may require specialized peak shape descriptions that are not presently implemented in Rietveld structure refinement computer codes. The simplicity of the TOFMANY code allows for straightforward modifications of the peak shape function used to fit the Bragg profiles. The minimization method does not require derivatives of the peak shape function. This means that functions which are not closed analytical expressions in a mathematical sense can be easily implemented in the program. For materials with very complicated crystal structures, the choice of techniques for structural refinement become severely limited. Analysis methods that rely on single peak or multiplet peak descriptions must be abandoned, but the Rietveld structure refinement technique is available. The success of this technique is well-known[1].

ACKNOWLEDGEMENTS

This work was supported by the U. S. Department of Energy, BES-Material Sciences under Contract W-31-109-Eng-38.

REFERENCES

1 IPNS Progress Report 1983-1985, Argonne National Laboratory, IPNS Division, Argonne, IL 60439 and references contained within. Proposal forms for experiments are also available.

2 G. H. Lander and D. L. Price, "Neutron Scattering with Spallation Sources", Phys. Today 38, 38 (1985).

3 J. M. Carpenter, G. H. Lander and C. G. Windsor, "Instrumentation at Pulsed Neutron Sources", Rev. Sci. Instrum. 55, 1019 (1984).

4 H. M. Rietveld, "A Profile Refinement Method for Nuclear and Magnetic Structures", J. Appl. Crystallogr. 2, 65 (1969).

5 R. B. Von Dreele, J. D. Jorgensen and C. G. Windsor, "Rietveld Refinement with Spallation Neutron Powder Diffraction Data", J. Appl. Crystallogr. 15, 581 (1982).

6 J. D. Jorgensen and F. J. Rotella, "High-Resolution Time-of-Flight Powder Diffractometer at the ZING-P' Pulsed Neutron Source", J. Appl. Crystallogr. 15, 27 (1982).

7 R. K. Crawford, R. T. Daly, J. R. Haumann, R. L. Hitterman, C. B. Morgan, G. E. Ostrowski and T. G. Worlton, "The Data Acquisition System for the Neutron Scattering Instruments at the Intense Pulsed Neutron Source", IEEE Trans. Nucl. Sci. NS-28, 3692 (1981).

8 J. R. Haumann, R. T. Daly, T. G. Worlton, and R. K. Crawford, "IPNS Distributed Processing Data Acquisition System", IEEE Trans. Nucl. Sci. NS28, 62 (1982).

9 J. Faber, Jr., "Sample Environments at IPNS: Present and Future Capabilities", Revue Phys. Appl. 19, 643 (1984).

10 J. D. Jorgensen and J. Faber, Jr., "Electronically Focussed Powder Diffractometers at IPNS-I", ICANS-VI Meeting, Argonne National Laboratory, June 27, 1982, ANL Report ANL-82-80, 105 (1983).

11 L. Koester and A. Steyerl, "Neutron Physics" in Springer Tracts in Modern Physics, 80, Springer-Verlag, NY 1977, pg 37.

12 S. R. MacEwen, J. Faber, Jr., and A. P. L. Turner, "The Use of Time-of-Flight Neutron Diffraction to Study Grain Interaction Stresses", Acta Metall. 31, 657 (1983).

13 B. A. Averill, S. M. Kauzlarich, B. K. Teo and J. Faber, Jr., "Structural and Physical Studies on a New Class of Low-Dimensional Conducting Materials: FeOCl Intercalated with TTF and Related Molecules", to be published in Molecular Crystals and Liquid Crystals, 1985.

14 A. D. Krawitz, R. Roberts and J. Faber, Jr., "Residual Stress Relaxation in Cemented Carbide Composites Studied Using the Argonne Intense Pulsed Neutron Source", Advances in X-Ray Analysis 27, University of Denver-Plenum Press, New York, 1984, pp 239-249.